Fluorescent Probes

Deutsche Ausgabe: DOI: 10.1002/ange.201507939
Internationale Ausgabe: DOI: 10.1002/anie.201507939

A Phosphole Oxide Based Fluorescent Dye with Exceptional Resistance to Photobleaching: A Practical Tool for Continuous Imaging in STED Microscopy

Chenguang Wang, Aiko Fukazawa, Masayasu Taki,* Yoshikatsu Sato, Tetsuya Higashiyama,* and Shigehiro Yamaguchi**

Abstract: *The development of stimulated emission depletion (STED) microscopy represented a major breakthrough in cellular and molecular biology. However, the intense laser beams required for both excitation and STED usually provoke rapid photobleaching of fluorescent molecular probes, which significantly limits the performance and practical utility of STED microscopy. We herein developed a photoresistant fluorescent dye C-Naphox as a practical tool for STED imaging. With excitation using either a $\lambda = 405$ or 488 nm laser in protic solvents, C-Naphox exhibited an intense red/orange fluorescence (quantum yield $\Phi_F > 0.7$) with a large Stokes shift (circa 5900 cm^{-1}). Even after irradiation with a Xe lamp (300 W, $\lambda_{ex} = 460$ nm, full width at half maximum (FWHM) = 11 nm) for 12 hours, 99.5 % of C-Naphox remained intact. The high photoresistance of C-Naphox allowed repeated STED imaging of HeLa cells. Even after recording 50 STED images, 83 % of the initial fluorescence intensity persisted.*

Super-resolution nanoscopic techniques, such as stimulated emission depletion (STED) microscopy, have evolved continuously over the past decade and have allowed scientists to visualize structural details in biological systems.[1–9] In STED imaging, a fluorescent dye is exposed to irradiation from two different laser sources, namely an excitation laser and a STED beam, where the STED beam is a donut-shaped beam for the depletion of excited molecules. The spatial resolution of STED imaging increases with the I_{STED}/I_{sat} ratio, where I_{STED} is the STED beam intensity and I_{sat} represents the saturation intensity at 50 % depletion.[10] An increase of the I_{STED} value, however, simultaneously accelerates the photobleaching of the dye, mainly through multiphoton absorption,[11] and even the most advanced photostable fluorophores currently available suffer from this limitation. Substantially enhancing the photostability of a fluorescent dye has therefore been a primary concern in order to employ STED microscopy for live imaging. Herein, we report promising fluorescent small molecules which exhibit outstanding photostability, even in living cells and under continuous STED imaging conditions, relative to currently available photostable fluorophores. This compound class is thus a powerful tool for the advancement of STED microscopy, with potential applications, for instance, in repeated time-lapse STED imaging and live video imaging.

Our molecular design was based on a core scaffold of (*N*,*N*-diphenylamino)phenyl-substituted benzophosphole *P*-oxide (Bphox; Figure 1),[12] which offers several distinct advantages as a fluorescent probe. First, the combination of the electron-donating properties of the amino moiety with the electron-accepting properties of the benzophosphole *P*-oxide leads to compounds with intense fluorescence emissions, which can retain high fluorescence quantum yields (Φ_F) even in polar and protic solvents. Second, this donor–acceptor combination gives rise to an intramolecular charge transfer (ICT) character of the excited state. This feature induces a large Stokes shift, which is advantageous in order to avoid autofluorescence interference and anti-Stokes excitation generated by the depletion laser. Third, upon increasing solvent polarity, the emission maximum undergoes a significant bathochromic shift, with the color of the emitted light changing from bluish green to reddish orange. Taking advantage of these features, we recently developed the corresponding 3-phenyl-substituted derivative Ph-Bphox and demonstrated its application as a polarity-sensitive probe.[12] To impart such scaffolds with high photostability, we designed structurally reinforced derivatives for this study, that is, the diarylmethylene-bridged (hereafter simply

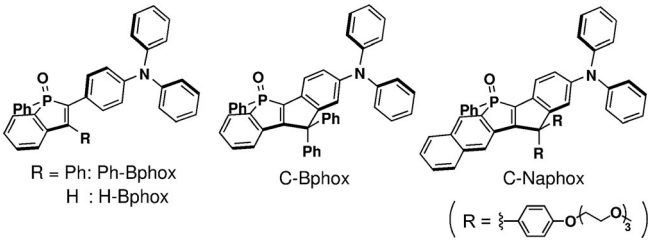

Figure 1. Molecular structures of fluorescent dyes based on phosphole *P*-oxides.

[*] Dr. C. Wang, Prof. Dr. M. Taki, Dr. Y. Sato, Prof. Dr. T. Higashiyama, Prof. Dr. S. Yamaguchi
Institute of Transformative Bio-Molecules (WPI-ITbM)
Nagoya University, Furo, Chikusa, Nagoya 464-8602 (Japan)
E-mail: taki@itbm.nagoya-u.ac.jp
higashi@bio.naogya-u.ac.jp
yamaguchi@chem.naogya-u.ac.jp
Prof. Dr. A. Fukazawa, Prof. Dr. S. Yamaguchi
Department of Chemistry, Graduate School of Science
Nagoya University, Furo, Chikusa, Nagoya 464-8602 (Japan)
E-mail: aiko@chem.nagoya-u.ac.jp
Prof. Dr. T. Higashiyama
Division of Biological Science, Graduate School of Science
Nagoya University, Furo, Chikusa, Nagoya 464-8602 (Japan)

Supporting information for this article is available on the WWW under http://dx.doi.org/10.1002/anie.201507939.

denoted as "carbon-bridged") benzophosphole and naphthophosphole *P*-oxides C-Bphox and C-Naphox (Figure 1). In the course of this study a nonbridged naphthophosphole derivative was reported by Matano and co-workers.[13]

These compounds were synthesized from the 3-bromo-substituted benzo- and naphthophosphole oxides **2a** and **2b** as key precursors, which were readily synthesized by the previously reported intramolecular *trans*-halophosphanylation of the corresponding phosphanyl-substituted diarylacetylenes (Scheme 1).[14] The reduction of **2a** and **2b** with $HSiCl_3$ followed by halogen–lithium exchange with *t*BuLi produced the corresponding lithiated intermediates. Subsequent treatment with diarylketones and a 30% H_2O_2 aqueous solution afforded 3-hydroxymethyl-substituted benzo- and naphthophosphole oxides **3a** and **3b**. Further intramolecular Friedel–Crafts cyclization in the presence of $BF_3{\cdot}OEt_2$ successfully gave the methylene-bridged molecules C-Bphox and C-Naphox in 65% and 48% yields, respectively. Triethyleneglycol chains were incorporated onto the carbon-bridged moiety in C-Naphox to increase its solubility, for which values of 1.0 and 0.10 g mL^{-1} were measured in dimethylsulfoxide (DMSO) and methanol (MeOH), respectively.

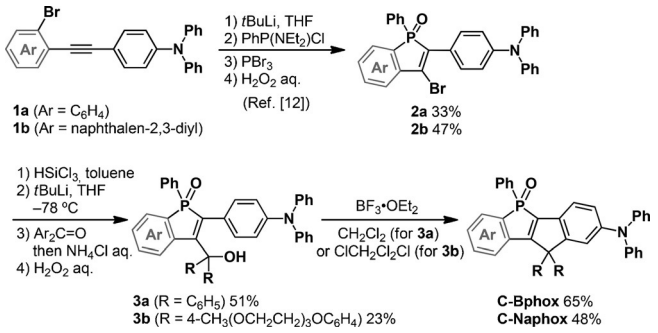

Scheme 1. Synthesis of C-Bphox and C-Naphox.

The photophysical properties for thus-prepared C-Bphox and C-Naphox were investigated in various solvents (Table 1; Figures S1 and S2 in the Supporting Information). In general, both compounds exhibit large Stokes shifts and substantial polarity-responsive fluorescence as a result of intramolecular charge transfer (ICT) character in the excited state. In comparison with Ph-Bphox, the bridged analogue C-Bphox shows a slightly red-shifted absorption band (circa 20 nm) because of more effective π conjugation, while the emission maximum wavelengths (λ_{em}) of C-Bphox are slightly blue-shifted relative to Ph-Bphox irrespective of solvent. As a result of the broad absorption bands of C-Bphox and C-Naphox centered around $\lambda = 425$–440 nm and tailing to 500 nm, excitation could not only be achieved using a $\lambda_{ex} = 405$ nm laser but also by a 488 nm laser, which are commonly used lasers in optical microscopy. In MeOH, C-Bphox and C-Naphox subsequently exhibited reddish-orange emission bands with maximum emission wavelengths of $\lambda = 608$ nm and 582 nm, respectively. The detected large Stokes shifts of 6400 cm^{-1} (C-Bphox) and 5900 cm^{-1} (C-Naphox) in MeOH should be a great advantage for fluorescent probes.[15]

Table 1: Photophysical data for benzophosphole-based fluorophores Ph-Bphox, C-Bphox, and C-Naphox in various solvents.

Compound	Solvents	λ_{abs} [nm][a]	ε [10^4 M^{-1} cm^{-1}]	λ_{em} [nm]	Φ_F[b]	τ [ns]	k_r [10^8 s^{-1}]	k_{nr} [10^8 s^{-1}]
Ph-Bphox	toluene	415	1.87	528	0.94	5.2	1.8	0.12
	CH_2Cl_2	415	1.73	565	0.90	7.3	1.2	0.14
	MeCN	404	1.59	597	0.61	7.0	0.87	0.56
	MeOH	415	1.53	613	0.22	2.9	0.76	2.7
C-Bphox	toluene	431	1.82	522	0.95	6.3	1.5	0.08
	CH_2Cl_2	434	1.69	564	0.92	8.8	1.0	0.09
	MeCN	427	1.70	594	0.81	8.7	0.93	0.22
	MeOH	438	1.60	608	0.40	6.1	0.66	0.98
C-Naphox	toluene	443	2.40	499	0.93	4.3	2.2	0.16
	CH_2Cl_2	431	2.48	543	0.93	6.1	1.5	0.11
	MeCN	424	2.45	570	0.88	6.8	1.3	0.18
	MeOH	433	2.32	582	0.71	7.1	1.0	0.41

[a] Longest wavelength absorption maximum. [b] Absolute fluorescence quantum yields determined with a calibrated integrating sphere system (errors < 3%).

It should be noted that the carbon-bridged and naphthalene-fused structure of C-Naphox is key for the generation of intense fluorescence, which gives rise not only to an increased molar extinction coefficient (ε) but also to substantially higher fluorescence quantum yields (Φ_F), even in polar and protic solvents. Whereas the Φ_F value of Ph-Bphox decreased from 0.61 in acetonitrile (MeCN) to 0.22 in MeOH, C-Naphox maintained a Φ_F value of 0.71 in MeOH. The fluorescence brightness, defined as the product between the ε and Φ_F values, for C-Naphox in MeOH was measured to be 1.65×10^4, which is 4.9 times higher than that of Ph-Bphox (3.37×10^3).

Studies on the excited-state dynamics revealed the impact of the carbon-bridged and naphthalene-fused structure on the fluorescence. Radiative (k_r) and nonradiative (k_{nr}) decay rate constants from the lowest excited singlet state (S_1) were determined based on the values for Φ_F and the fluorescence lifetime (τ; Table 1 and Figure S3). In MeOH, both C-Naphox and C-Bphox exhibited significantly smaller k_{nr} values relative to that of Ph-Bphox, demonstrating a significant impact of structural rigidity on the suppression of nonradiative decay. Conversely, the higher k_r value detected for C-Naphox compared to C-Bphox demonstrated that the expansion of the π conjugation with the naphthalene skeleton accelerates the radiative decay from the excited state, but does not cause a bathochromic shift of the emission wavelength. The synergistic effect between these two factors should thus be responsible for the high brightness of C-Naphox.

The ICT character of the fluorescent molecule is sometimes affected by environmental pH values. Before staining cells with C-Naphox, we measured fluorescence spectra in

a mixture of DMSO and pH buffer solution (7:3 v/v; pH 1–11). The emission spectra of C-Naphox remained unchanged for a wide range of pH values (Figure S4). Because the conjugate acid of triphenylamine moiety has a pK_a value of −5, no protonation occurs on the amino group in the biological pH range.

Cytotoxicity of the fluorescent probe is another important issue for staining living cells. A cytotoxic MTT assay of C-Naphox in HeLa cells was conducted with an incubation period of 24 h (37 °C, 5 % CO_2). No significant cytotoxicity, that is about 100 % cell viability, was detected for concentrations up to 10 μM (Figure S7). This result indicates that sub-μM concentrations of C-Naphox, which are usually required for cellular staining experiments, can be used for prolonged imaging experiments in live cells.

C-Bphox and C-Naphox were found to exhibit exceptionally high resistance to photobleaching. The photostabilities of Ph-Bphox, C-Bphox, and C-Naphox were initially examined in MeCN solution under irradiation with a pulsed laser (λ_{ex} = 405 nm, 55 ps, 273 mW, 100 MHz; Figure 2a). Ph-Bphox has higher stability in comparison with the corresponding protonated derivative H-Bphox, demonstrating that the presence of the phenyl group already substantially enhances the photostability. An even more pronounced improvement was detected for the structurally reinforced derivatives C-Bphox and C-Naphox, both of which did not show any significant photobleaching even after continuous exposure to irradiation from the λ_{ex} = 405 nm laser for 2 hours. As photobleaching may potentially arise from reaction at the central double-bond moiety with singlet O_2 and/or a hydroxyl radical generated during photoexcitation, the protection of this double bond by the phosphoryl moiety and the carbon bridge should thus effectively prevent those degradation processes.

To highlight the photostability of C-Naphox, the compound was compared to the representative STED imaging probes Alexa Fluor 488 (Alexa 488) and Atto 488 (see the Experimental Section) in DMSO/HEPES buffer (7:3 v/v, pH 7.3; HEPES = 2-[4-(2-hydroxyethyl)-1-piperazinyl]ethanesulfonic acid) under irradiation with a Xe lamp (300 W) equipped with a band-pass filter of λ_{ex} = 460 nm (half peak width = 11 nm). After irradiation for 2 h, although 26.2 % of Alexa 488 and 96.7 % of Atto 488 persisted, 99.9 % of C-Naphox remained intact. Even after irradiation for 12 h, during which only 58.7 % of Atto 488 persisted, C-Naphox still remained almost quantitatively intact (99.5 %; Figure 2b, Figure S5). A more pronounced difference was detected upon irradiation with a Xe lamp (300 W) using a cut-off filter of λ_{ex} > 325 nm (Figure S6). After 70 min of irradiation, 99.5 % of C-Naphox remained, whereas only 35 % of Atto 488 persisted. These results clearly demonstrated the excellent photostability of the structurally reinforced derivatives, at least in terms of the photoexcitation from the ground state (S_0) to the first singlet excited state (S_1) and the corresponding decay from the S_1 to S_0 state.

The outstanding photostability of C-Naphox encouraged us to employ it for fluorescence imaging in STED microscopy. To evaluate the performance of the compound as a fluorescent probe in biological samples, confocal images of living

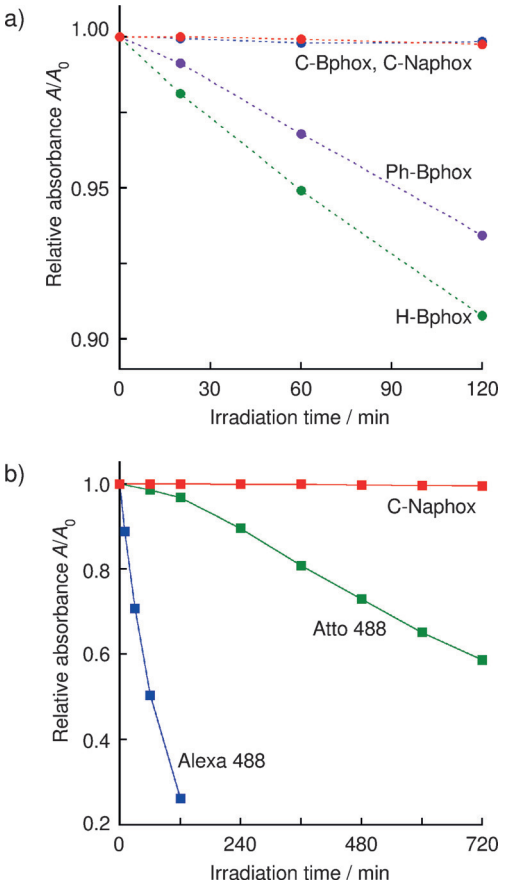

Figure 2. Photostability of the phosphole oxide based fluorescent dyes. a) Relative absorbance values of Ph-Bphox (purple circle), H-Bphox (green circle), C-Bphox (blue circle), and C-Naphox (red circle) as a function of irradiation time with a 405 nm pulse laser in MeCN solutions. b) Relative absorbance values of DMSO/HEPES buffer solutions (pH 7.3, 7:3 v/v) of C-Naphox (red square), Alexa 488 (blue square), and Atto 488 (green square) as a function of irradiation time, after irradiation with a Xe lamp (300 W) using a band-pass filter of 460 ± 11 nm. In all cases, solution concentrations were adjusted to be comparable in terms of optical density at 405 nm and 460 nm for (a) and (b), respectively. A_0 = absorbance at t = 0.

HeLa cells stained with C-Naphox were taken initially using a Leica TCS STED CW microscope (Leica Microsystems; CW = continuous wave). A fluorescence image of an entire cell (Figure 3; Figure S8) demonstrated that the dye was membrane permeable and distributed in intracellular network structures. Its staining pattern partially overlapped with that of an Alexa 488-conjugated anti-KDEL antibody, a commercially available endoplasmic reticulum (ER) marker, suggesting that hydrophobic C-Naphox prefers to accumulate in hydrophobic organelles such as the ER (Figure S9). However, nonspecific binding of the dye could not be eliminated even after repeated washings of the cells with phosphate buffered saline (PBS; pH 7.0). STED imaging of the same cell (Figure S8a) using an excitation laser of λ_{ex} = 488 nm and an STED depletion laser of λ_{ex} = 592 nm, provided a high-resolution image (Figure S8b).

To evaluate the potential of C-Naphox as a fluorescent labeling reagent for repeated and prolonged STED imaging, its intracellular photostability under STED conditions was

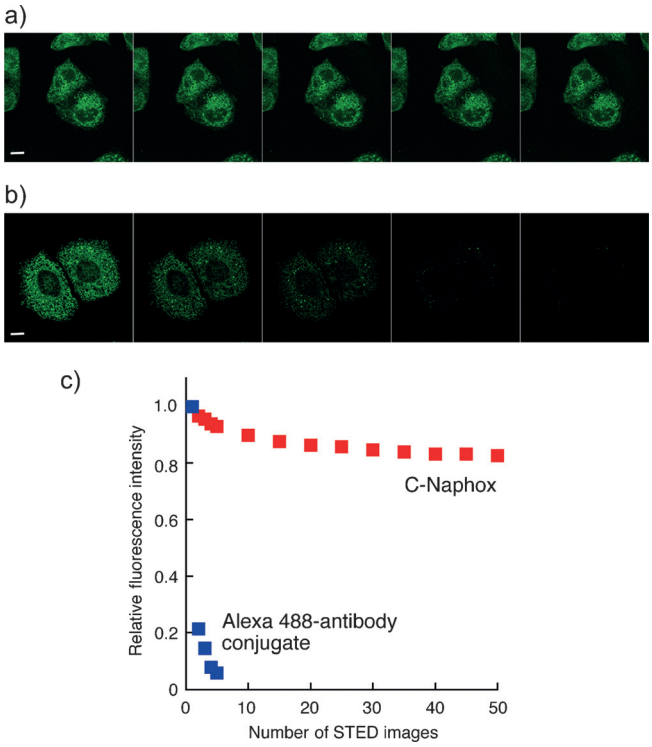

Figure 3. Comparison of the photostabilities of C-Naphox and an Alexa 488-antibody conjugate in fixed HeLa cells under STED conditions. Repeated STED images of cells stained with a) C-Naphox and b) the Alexa 488-conjugated anti-KDEL antibody. After the stained cells were mounted on the microscope stage, five images were taken consecutively at 2 min 45 sec intervals. Irradiation sources: a tunable white-light excitation laser (488 nm, 80 MHz, output power 70%, AOTF 80%) and a CW-STED laser (592 nm CW laser, output power 95%, AOTF 100%). c) Plots of normalized intracellular fluorescence intensity as a function of the number of recorded STED images. Normalization was carried out against the initial fluorescence intensity. Scale bars in (a, b) = 10 μm.

compared to that of antibody-conjugated Alexa 488. After fixing and staining the cells with each dye, the imaging experiments were carried out using a $\lambda = 488$ nm excitation laser (white light laser, output power 70%, AOTF 80%; AOTF = acousto-optic tunable filter) and a 592 nm STED beam (CW laser, output power 95%, AOTF 100%). Most importantly, the intensity of the C-Naphox fluorescence signal remained virtually unchanged, even after recording five images (Figure 3a), whereas a significant decrease in signal intensity was detected for cells labelled with Alexa 488 during the measurement (Figure 3b). This is particularly noteworthy considering that Alexa 488 is currently regarded as one of the most photoresistant commercially available dyes. Moreover, the intracellular fluorescent intensity of C-Naphox remained at 83% of the initial value even after recording 50 images using identical laser intensities (Figure 3c). To our knowledge, C-Naphox is thus the first fluorescent dye that permits repeated STED imaging at such a low degree of photodegradation.[16]

In summary, we have developed a bright and highly photostable fluorescent dye, C-Naphox, by the incorporation of a carbon bridge into the naphthophosphole *P*-oxide fluorophore. In contrast to previously reported photostable dyes, such as Alexa 488 and Atto 488, C-Naphox exhibited superior photostability under STED conditions. By using C-Naphox, we successfully achieved repeated STED imaging of HeLa cells without suffering serious photobleaching even after a 50-fold repetition. The enhancement of the fluorophore stability under STED imaging conditions is absolutely imperative for the practical application of STED imaging in the visualization of various biological events. The remarkable photostability of C-Naphox should thus open a previously unattainable avenue to record prolonged live STED imaging, potentially enabling the visualization of various biological events with high spatial resolution.[17] The polarity-responsive fluorescence with large Stokes shifts should impart C-Naphox with the potential for multi-color imaging and thus increase its value even further.

Experimental Section

Evaluation of photostability: The photostability of the fluorophores was evaluated by considering both the variation of the absorption of each sample at the absorption maximum wavelength (λ_{abs}) and the irradiation time upon irradiation of the sample with laser light or using a Xe lamp. To compare the photostability of the fluorophores Ph-Bphox, H-Bphox, C-Bphox, and C-Naphox (Figure 3a), a picosecond light pulser (frequency 100 MHz; C10196, Hamamatsu Photonics) with a laser diode head of $\lambda = 405$ nm (pulse width 55 ps, maximum output power 273 mW; PLP10-040, Hamamatsu Photonics) was used. The sample solution in MeCN in a quartz cuvette was irradiated at room temperature under identical irradiation conditions in terms of the distance and output power of the laser. The concentrations of the sample solution were adjusted to be comparable to one another in terms of optical densities (0.39 of Ph-Bphox, 0.43 of H-Bphox, 0.42 of C-Bphox, and 0.39 of C-Naphox) at the excitation wavelength of $\lambda = 405$ nm. The absorption spectra of each sample were measured at 0, 20, 60, and 120 min during the irradiation. To compare the photostability of C-Naphox and representative dyes, a 300 W Xe lamp (Asahi spectra, MAX-302) equipped with a $\lambda = 460$ nm band-pass filter (a half peak width of 11 nm) was used. The sample solutions of C-Naphox, Alexa 488 (Alexa Fluor 488 Hydrazide, Life technologies), and Atto 488 (Atto 488 NHS ester, Sigma–Aldrich) were prepared in a mixture of DMSO and HEPES buffer (pH 7.3) with a volume ratio 7:3 v/v. Their concentrations were adjusted to be comparable to one another in terms of optical densities (0.21 of C-Naphox, 0.22 of Alexa 488, and 0.22 of Atto 488) at the excitation wavelength of $\lambda = 460$ nm. The sample solution in a quartz cuvette was placed at a distance of 3.5 cm from the Xe light source. The absorption spectra were measured at appropriate times during the irradiation.

STED imaging: Super resolution microscopy was performed using the TCS SP8 STED with a HCXPL APO 100x/1.40 oil immersion lens (Leica). In live-cell imaging stained by C-Naphox, the emission spectrum at $\lambda = 495$–590 nm was collected using a 488 nm laser line (Ar laser; output power 30%, AOTF 80%) and a STED depletion laser line (592 nm CW laser; output power 95%, AOTF 95%) were used. For continuous STED imaging, the fixed cells stained by anti-KDEL antibody conjugated with Alexa 488 or C-Naphox were excited with a 488 nm laser line (white light laser; 80 MHz, output power 70%, AOTF 80%) and a STED laser (592 nm CW laser; output power 95%, AOTF 100%). The emission spectrum at $\lambda = 495$–585 nm was collected in 2 min 45 sec intervals. For the evaluation of photostability, total fluorescence intensities of the region of interest (ROI) were normalized to the ROI in the first images, and the relative intensities were plotted against the number of STED images.

Acknowledgements

We would like to thank N. Sugimoto (Nagoya Univ.) for supporting cell biological experiments and Prof. Dr. N. Sasaki and T. Sasaki (Nagoya Univ.) for providing HeLa cells. This work was partly supported by the JST, CREST (S.Y.), and the Japan Advanced Plant Science Network. ITbM is supported by the World Premier International Research Center (WPI) Initiative, Japan.

Keywords: fluorescent probes · phosphorus heterocycles · photophysics · photoresistance · STED microscopy

How to cite: *Angew. Chem. Int. Ed.* **2015**, *54*, 15213–15217
Angew. Chem. **2015**, *127*, 15428–15432

[1] K. I. Willig, F. J. Barrantes, *Curr. Opin. Chem. Biol.* **2014**, *20*, 16–21.
[2] L. Schermelleh, R. Heintzmann, H. Leonhardt, *J. Cell Biol.* **2010**, *190*, 165–175.
[3] M. Fernández-Suárez, A. Y. Ting, *Nat. Rev. Mol. Cell Biol.* **2008**, *9*, 929–943.
[4] T. Müller, C. Schumann, A. Kraegeloh, *ChemPhysChem* **2012**, *13*, 1986–2000.
[5] C. Eggeling, K. I. Willig, F. J. Barrantes, *J. Neurochem.* **2013**, *126*, 203–212.
[6] R. S. Erdmann, H. Takakura, A. D. Thompson, F. Rivera-Molina, E. S. Allgeyer, J. Bewersdorf, D. Toomre, A. Schepartz, *Angew. Chem. Int. Ed.* **2014**, *53*, 10242–10246; *Angew. Chem.* **2014**, *126*, 10407–10412.
[7] B. Hein, K. I. Willig, S. W. Hell, *Proc. Natl. Acad. Sci. USA* **2008**, *105*, 14271–14276.
[8] G. Lukinavičius, K. Umezawa, N. Olivier, A. Honigmann, G. Y. Yang, T. Plass, V. Mueller, L. Reymond, I. R. Corrêa, Z. G. Luo, C. Schultz, E. A. Lemke, P. Heppenstall, C. Eggeling, S. Manley, K. Johnsson, *Nat. Chem.* **2013**, *5*, 132–139.
[9] G. Lukinavičius, L. Reymond, E. D'Este, A. Masharina, F. Gutfert, H. Ta, A. Guether, M. Fournier, S. Rizzo, H. Waldmann, C. Blaukopf, C. Sommer, D. W. Gerlich, H. D. Arndt, S. W. Hell, K. Johnsson, *Nat. Methods* **2014**, *11*, 731–733.
[10] T. A. Klar, S. Jakobs, M. Dyba, A. Egner, S. W. Hell, *Proc. Natl. Acad. Sci. USA* **2000**, *97*, 8206–8210.
[11] M. Dyba, S. W. Hell, *Appl. Opt.* **2003**, *42*, 5123–5129.
[12] E. Yamaguchi, C. G. Wang, A. Fukazawa, M. Taki, Y. Sato, T. Sasaki, M. Ueda, N. Sasaki, T. Higashiyama, S. Yamaguchi, *Angew. Chem. Int. Ed.* **2015**, *54*, 4539–4543; *Angew. Chem.* **2015**, *127*, 4622–4626.
[13] Y. Matano, Y. Motegi, S. Kawatsu, Y. Kimura, *J. Org. Chem.* **2015**, *80*, 5944–5950.
[14] A. Fukazawa, Y. Ichihashi, Y. Kosaka, S. Yamaguchi, *Chem. Asian J.* **2009**, *4*, 1729–1740.
[15] H. Schill, S. Nizamov, F. Bottanelli, J. Bierwagen, V. N. Belov, S. W. Hell, *Chem. Eur. J.* **2013**, *19*, 16556–16565.
[16] K. Kolmakov, C. A. Wurm, R. Hennig, E. Rapp, S. Jakobs, V. N. Belov, S. W. Hell, *Chem. Eur. J.* **2012**, *18*, 12986–12998.
[17] J. Requejo-Isidro, *J. Chem. Biol.* **2013**, *6*, 97–120.

Received: August 25, 2015
Published online: October 23, 2015